

Cluster virial expansion of the equation of state for hydrogen plasma with e -H₂ contributionsY. A. Omarbakiyeva,^{1,2,*} H. Reinholz,^{1,3} and G. Röpke¹¹*Institute of Physics, University of Rostock, D-18051 Rostock, Germany*²*International IT University, 050040 Almaty, Kazakhstan*³*The University of Western Australia, Crawley, Western Australia 6009, Australia*

(Received 23 July 2014; published 20 April 2015)

The equation of state of partially ionized hydrogen plasma is considered with special focus on the contribution of the e -H₂ interaction. Traditional semiempirical concepts such as the excluded volume are improved using microscopic approaches to treat the e -H₂ problem. Within a cluster virial expansion, the Beth-Uhlenbeck formula is applied to infer the contribution of bound and scattering states to the temperature-dependent second virial coefficient. The scattering states are calculated using the phase expansion method for the polarization interaction that incorporates experimental data for the e -H₂ scattering cross section. We present results for the scattering phase shifts, differential scattering cross sections, and the second virial coefficient due to the e -H₂ interaction. The influence of this interaction on the composition of the partially ionized hydrogen plasma is confined to the parameter range where both the H₂ and the free-electron components are abundant.

DOI: [10.1103/PhysRevE.91.043103](https://doi.org/10.1103/PhysRevE.91.043103)

PACS number(s): 52.25.Kn, 52.20.Hv

I. INTRODUCTION

The equation of state (EOS) describes the equilibrium properties of matter, including the charge-neutral plasmas considered here. At present, it attracts significant attention of researchers working in different fields.

For instance, the calculation of thermodynamic properties of plasmas in the warm dense matter (WDM) region is necessary to model the planetary and stellar interiors [1,2]. With the extension of the plasma parameter region to the condensed matter densities and temperatures up to several rydbergs, it is now possible to describe the composition of the giant planets such as Jupiter and Saturn [3–6]. High-energy-density physics is another field where the WDM equation of state is of interest [7]. In particular, the hydrogen EOS is of relevance for inertial confinement fusion [8]. Although these applications concern systems in nonequilibrium to be described, for instance, by kinetic theory, the equation of state of WDM based on equilibrium properties such as temperature, chemical potential, and composition is an important ingredient in the understanding of the microscopic state of these systems. In the astrophysics of compact objects, the use of a hydrodynamic description is justified because WDM is strongly coupled so that the relaxation to a local thermodynamic equilibrium is sufficiently quick.

Thermodynamic equilibrium is described by the grand canonical ensemble. Within the quantum statistical approach to the EOS, numerical techniques such as density-functional theory and quantum molecular dynamics simulations have been elaborated [9]. Correlations and bound-state formation are of relevance. Simple treatments of plasma using perturbation methods are not able to describe, for instance, the formation of bound states. In particular, nonideal contributions are involved due to the interaction between charged and neutral particles, which can be treated within either the chemical picture where bound states are considered as new components or the physical picture where the elementary components (electrons and ions)

are considered and the bound states are formed due to the interaction.

In the chemical picture (see [10–14]), the plasma is assumed to consist of well-defined reacting particles: electrons, ions, atoms, and molecules. The simple chemical picture that considers an ideal mixture of the different components is valid only in the low-density limit. With increasing density, the interaction between the constituents gives a contribution to the thermodynamic equation of state. However, systematic quantum statistical approaches [10,13] allow us to investigate a wide range of thermodynamic parameters, avoiding inconsistencies such as double-counting effects.

Interactions are described via effective short-range potentials for neutral particles and long-range potentials between charged particles (see [10,13]). The thermodynamic characteristics of nonideal plasma can be represented by the free energy, which is calculated on the basis of different pseudopotential models for a certain pair interaction. Usually, the nonideal part of the free energy is considered to consist of the contributions for Coulomb interactions (electron-electron, ion-ion, and ion-electron), polarization interactions between charged and neutral particles, and short-range interactions between neutrals. This model has been successfully applied [11,12,14] to investigate properties of partially ionized plasmas.

In the physical model, the fundamental structural elements are the electrons and protons with Coulomb interactions. The composite particles i.e., atoms, molecules, and other heavier components, are obtained from few-body wave equations. The latter are assumed to consist of fundamental particles and their properties should be determined by solving the corresponding Schrödinger equation. Within the physical picture, virial expansions (with respect to density or fugacity) have been evaluated [15]. In the density virial expansion, the second virial coefficient is determined by pair interactions. Interactions of electrons with the neutral composite particles appear in higher orders (third virial coefficient, etc.). Alternatively, the contribution of neutral particles can be taken into account within a cluster virial expansion. In the fugacity expansion, the formation of bound states (clusters) is consistently included. For instance, in the low-density limit two-particle bound states

*yultuz.omarbakiyeva@uni-rostock.de

are stable. Therefore, it is possible to consider the bound states as new particles. We switch from the physical picture to the chemical picture, which means the partial summation of ladder diagrams that describes the formation of bound states with a Green's function approach. The three-particle interaction in the physical picture will be considered as effective two-particle interaction in the chemical picture after inclusion of cluster states. An alternative to treating the physical model beyond any perturbation expansions is path-integral Monte Carlo simulation (see [16]). Attempts to understand the results in terms of a composition including atoms and molecules are defined by semiempirical cutoff radii.

The cluster virial expansion was described in details in a previous paper [17]. The electron-atom interaction was studied from a microscopic point of view. Different pseudopotentials were compared and empirical data for separable potentials were given. With the help of the Beth-Uhlenbeck formula [18], it was shown that the second virial coefficient in the electron-atom channel is related to scattering phase shifts as well as bound states. In contrast to previous approaches, results for the second virial coefficient in the e -H channel were not based on any pseudopotential models, but were directly derived from measured scattering data. Simultaneously, the contribution of the bound state H^- was included. The use of experimental data as an input for the Beth-Uhlenbeck formula avoids any empirical parameters and may be considered as a low-density benchmark for any equation of state. In this present work, this approach will be extended to include further components of the plasma, in particular H_2 molecules interacting with electrons.

We study partially ionized hydrogen plasma with electrons (e), ions (protons i), hydrogen atoms (H), and hydrogen molecules (H_2) as constituents starting from the chemical picture. We focus on the interaction of e - H_2 and its contribution to the equation of state. The influence of the molecular component is essential in dense partially ionized plasmas. The composition of hydrogen plasma has been calculated following a set of mass action laws [10]. Figure 1 presents a standard approach [10] to the composition of hydrogen plasma, exemplarily for $T = 15\,000$ K, with particle densities fractions $\alpha_c = Z_c n_c / n_e^{\text{tot}}$, where n_c is the density of species c , n_e^{tot} is the total electron density, and Z_c is the number of electrons in the corresponding bound states. The free-electron-density fraction is decreasing until total electron densities of 10^{23} cm^{-3} before pressure ionization sets in. The fraction of hydrogen atoms dominates in the density region $\approx 10^{18}$ – 10^{24} cm^{-3} . At densities above 10^{21} cm^{-3} , the molecule fraction plays an essential role in physical processes. Note that, following [10], the interactions between electrons and clusters are not taken into account to calculate the composition in Fig. 1. The use of experimental data for the interaction parts of chemical potentials can give more accurate data for the composition. In the present work, we consider partially ionized hydrogen plasmas at temperatures $T \leq 10^5$ K and densities up to 10^{22} cm^{-3} until degeneracy effects play an essential role. Another ingredient, the contribution of scattering states, is considered. We apply the cluster virial expansion approach to study the contribution of the electron-molecule interaction to thermodynamical properties. The present work is organized as follows. In Sec. II we briefly review the cluster virial expansion and the Beth-Uhlenbeck formula for the second

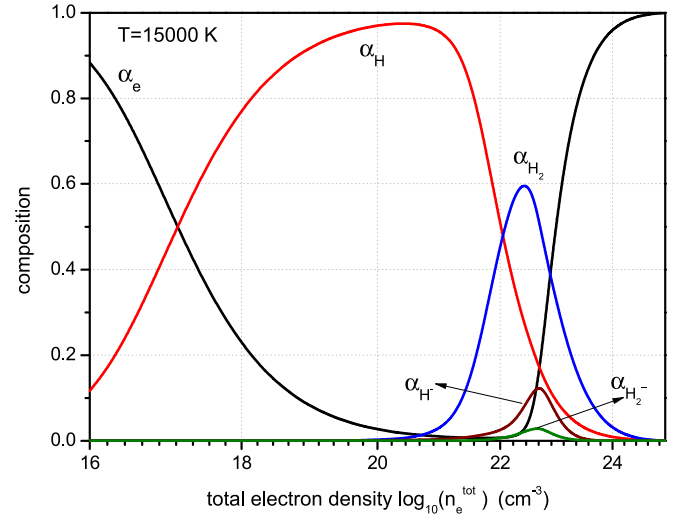


FIG. 1. (Color online) Composition of hydrogen plasma at $T = 15\,000$ K using mass action laws [10]. Particle-density fractions of electrons, hydrogen atoms, hydrogen molecules, negative hydrogen ions, and molecular ions are shown. Interaction between electrons and bound states are not taken into account.

virial coefficient. Section III contains the calculation of the scattering phase shifts for the electron-molecule system, via both experimental differential cross sections and phase shifts from appropriate pseudopotentials. In Sec. IV the phase shifts are used to calculate the corresponding second virial coefficient. Results for the H_2 - e second virial coefficient are given for different temperatures and consequences for the composition are considered. A summary is given and conclusions are drawn in Sec. V.

II. CLUSTER VIRIAL EXPANSION AND BETH-UHLENBECK FORMULA

The cluster virial expansion for the equation of state [19] can be written as a function of fugacities $z_c = e^{\beta(\mu_c - E_c^{(0)})}$,

$$\beta p = \sum_c \frac{2s_c + 1}{\Lambda_c^3} \left(z_c + \sum_d z_c z_d \tilde{b}_{cd} + \dots \right), \quad (1)$$

where c denotes species ($c = e, i, H, H_2$), s_c spin, μ_c chemical potential, $E_c^{(0)}$ binding energy for isolated cluster species, and $\Lambda_c = (2\pi\hbar^2/k_B T m_c)^{1/2}$ the thermal wavelength of species c . The first term is the ideal part of the pressure. The contribution of the Coulomb interaction between charged particles and the interaction with neutrals must be treated differently. For the Coulomb interactions ($e - e$, $e - i$, and $i - i$), the nonideal contributions of the equation of state have been intensively investigated (for a review see Ref. [13]). For the interaction with neutrals, the dimensionless second virial coefficient \tilde{b}_{cd} is determined by the respective interactions of e -H, i -H, H-H, e - H_2 , i - H_2 , H_2 - H_2 , and H- H_2 pairs. In particular, \tilde{b}_{H-H} was calculated in Ref. [20] and \tilde{b}_{e-H} was studied in Ref. [17].

TABLE I. Contribution of various transitions to total e -H₂ scattering cross sections a_B^2 at different impact energies.

Transition	7	10	13.6	20	45	60	81.6
total scattering ^a	42.1	33.7	26.9	20.0			
electronic excitation ^b	0.0	0.73	3.27	5.23			
total scatt. – electronic exc.	42.1	33.0	23.6	14.8			
elastic scattering ^b	41.5	32.6	23.4	14.7	7.86	5.97	4.44
vibrational excitation ^b	0.60	0.35	0.11	0.05	0.05	0.03	0.03

^aReference [24].^bReference [23].

An exact quantum mechanical expression for the second virial coefficient was given by Beth and Uhlenbeck [19]:

$$\tilde{b}_{cd} = \sum_{\ell} (2\ell + 1) \sum_n (e^{-\beta E_{cd}^{n\ell}} - 1) + \sum_{\ell=0}^{\infty} (2\ell + 1) \frac{\beta}{\pi} \int_0^{\infty} e^{-\beta E} \eta_{\ell}^{cd}(E) dE, \quad (2)$$

where ℓ is orbital momentum, $\eta_{\ell}^{cd}(E)$ is the scattering phase shift, E is the energy of incident particles, and $E_c^{n\ell}$ is binding energy of the state with quantum numbers $n\ell$. The first term is the bound part $\tilde{b}_{cd}^{\text{bound}}$ and the second is the scattering part $\tilde{b}_{cd}^{\text{sc}}$.

In this paper we focus on the second virial coefficient for e -H₂. We calculate the scattering part of the second virial coefficient \tilde{b}_{H_2-e} due to the electron-hydrogen molecule interaction. The bound part includes a new component H₂⁻ in the system. The calculation of the bound part requires the binding energy of the negative hydrogen molecule, which was taken from the literature [21]. Note that alternatively to Eq. (2), the bound state H₂⁻ can be considered as a new species c in calculating thermodynamic properties.

III. SCATTERING DATA

Scattering phase-shift data for e -H₂ can be employed to calculate the second virial coefficient \tilde{b}_{H_2-e} using the Beth-Uhlenbeck formula (2). Due to the internal degrees of freedom of the H₂ molecule, the e -H₂ scattering problem is more complex compared to the e -H system. In addition to electronic excitation and ionization, other processes have to be considered. Here we assume that the maximum energies of the incident electrons are below the ionization limit $E_i = 124\,417.49 \text{ cm}^{-1} \approx 15.42 \text{ eV}$ [22]. Then the total cross section Q_T includes the following contributions:

$$Q_T = Q_{\text{elas}} + Q_{\text{att}} + Q_{\text{diss}} + \sum Q_{\text{excit}}, \quad (3)$$

where the cross section for elastic scattering is Q_{elas} , that for dissociative attachment is Q_{att} , and that for impact dissociation is Q_{diss} . In addition, $\sum Q_{\text{excit}}$ is the sum of all excitation cross sections of rotational, vibrational, and electronic states. Table I shows the contribution of those transitions, which were estimated in Ref. [23]. The rotational excitation is not given. However, this channel is mixed into elastic and vibrational excitation transitions. As can be seen in Table I, the electronic excitation channel is closed until 7 eV. At 7 eV the vibrational transitions contribute about 1.4% to the

total cross section, which decreases with increasing incident energy. Up to 10 eV the total cross section is dominated by elastic contributions. This statement is further verified by considering the collision cross sections (see Fig. 2). Data were taken from Ref. [25], where a complete set of cross sections was presented including rotational, vibrational, and electronic excitation processes as well as dissociative attachment. Note that Q_{rot} is determined from theoretical data of Ref. [26]. The most important processes in the low-energy region are elastic scattering (momentum transfer) and rotational and vibrational excitations. The most accurate data were obtained in a swarm analysis due to Crompton and co-workers [26,27]. The rotational excitation channel is already open at $44 \times 10^{-3} \text{ eV}$ for the lowest rotational state ($J = 0 \rightarrow 2$). Therefore, experimental data for elastic differential cross sections would include rotational excitations that show a large number of possible states, even rotational-vibrational excitations [26,27]. Only in the experiment by Linder and Schmidt [28] was elastic scattering separated from rotational excitations. The vibrational channel sets in at 0.516 eV and the electronic excitation channel at 7 eV. However, the contributions of electronic, rotational, and vibrational excitations to the total cross section below 10 eV are not more than 1.04%, 10%, and 2.89%, respectively. According to our discussion above, the vibrational and rotational contributions in the total cross

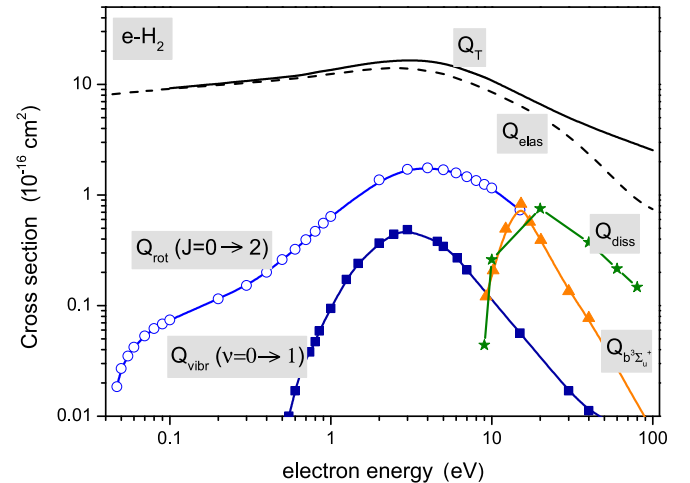


FIG. 2. (Color online) Cross section for e -H₂ collision due to different scattering channels: Q_{elas} , elastic scattering; Q_{diss} , impact dissociation; Q_{rot} , rotational excitations; Q_{vibr} , vibrational excitations; and $Q_{b^3\Sigma_u^+}$, electronic excitations, adapted from Ref. [25].

section of the e -H₂ scattering can be neglected. We consider only elastic contributions for our further calculations.

A. e -H₂ scattering theory

Various theoretical methods were developed to solve the Schrödinger equation for the e -H₂ scattering process. The T -matrix expansion method, the Schwinger variational method, and the R -matrix method are so-called basis-set expansion methods applied for the electron-molecule system (see the detailed review of theoretical methods in Ref. [29]). An alternative approach is a one-particle picture for the description of the elastic scattering process in the fixed-nucleus (Born-Oppenheimer) limit [29]. Molecules are fixed in position and the Schrödinger equation is solved for the electrons in the static electric potential arising due to the molecular configuration.

In low-energy limit, it is possible to use the modified effective range theory (MERT) for the scattering of an electron on a neutral polarizable system. The MERT was first developed and applied by O'Malley *et al.* in Refs. [30,31]. Recently, the applicability of the MERT for electron and positron elastic scattering on molecular targets was investigated in Ref. [32]. Instead of the traditional MERT, the exact analytical solutions of the Schrödinger equation for the long-range polarization potential was used. This extends the applicability of the MERT up to a few eV regime. Using the recommended total-cross-section data for the hydrogen molecule [33], fit parameters for the MERT model were found. Good agreement with experimental data was achieved using only two partial waves (s and p waves).

In this paper we solve the scattering problem of the electron-hydrogen molecule system assuming that molecules are fixed in space and are neither rotating or vibrating. In this case, the interaction between an electron and a molecule is treated similarly to that of an electron-atom system. That means that the electron is scattered by an optical potential V ,

$$H_{\text{eff}} = T_e + V, \quad (4)$$

and we use the phase function method [34,35] to solve the Schrödinger equation.

The phase function equation or so-called Calogero equation for the scattering phase shift η_ℓ is

$$\frac{d\eta_\ell^{cd}(k,r)}{dr} = -\frac{1}{k}U(r)\left[\cos\eta_\ell^{cd}(k,r)J_\ell(k,r) - \sin\eta_\ell^{cd}(k,r)n_\ell(k,r)\right]^2 \quad (5)$$

(for more details see Ref. [36]). The Calogero equation is solved for an initial condition $\eta_\ell^{cd}(k,0) = 0$, where k is the wave number, ℓ are orbital quantum numbers, $J_\ell(k,r)$ and $n_\ell(k,r)$ are the Riccati-Bessel functions, $U(r) = \frac{2m_e}{\hbar^2}V(r)$, and $V(r)$ is the interaction potential. The energy-dependent scattering phase shifts $\eta_\ell^{cd}(k)$ are determined as $\eta_\ell^{cd}(k) = \lim_{r \rightarrow \infty} \eta_\ell^{cd}(k,r)$.

B. Interaction potential

As we mentioned above, the accurate calculation of the scattering problem requires an adequate approximation of the optical potential. It is a full projectile-target (electron-molecule) interaction potential that consists of static, ex-

change, and polarization contributions. The static potential is given by the electrostatic interaction between the projectile and the constituent particles of the target [26]. The exchange effect is important at low energies; it occurs due to the indistinguishability of the projectile and target electrons. The polarization potential describes induced distortions of the target by the impact electron. Since the goal is to consider a collision process in plasma, the last effect (polarization) is particularly important for the description of plasma properties. Collisions of electrons on molecules in plasmas with not too high densities occur at large distances. The polarization potential for the electron-atom interaction has the asymptotic behavior $\alpha/2r^4$ (at large distances) with the polarizability α of the atom. Since this potential is diverging at small distances, the Buckingham potential was suggested for the e - a interaction [37]

$$V_{e-a} = -\frac{\alpha}{2(r^2 + r_0^2)^2}, \quad (6)$$

where r_0 is a cutoff radius. For hydrogen atoms $\alpha = 4.5a_B^3$ and $r_0 = 1.456a_B$ [38]. If we consider the interaction of electrons with diatomic molecules, the polarization model is modified [26,29]:

$$V_{e-H_2}(r) = \left(-\frac{\alpha_0}{2r^4} - \frac{\alpha_2}{2r^4}P_2(\cos\theta_p) \right) \times [1 - \exp(-r/r_0)^6], \quad (7)$$

where α_0 and α_2 are polarizabilities parallel and perpendicular to the internuclear axis \vec{e}_R , respectively, $P_2(\cos\theta_p)$ is the Legendre polynomial, and θ_p is the angle between the direction of the incident electron and the z axis. This potential describes the interaction of a molecule positioned at the origin and the z axis coincides with \vec{e}_R . For H₂ (internuclear distance $R = 1.4a_B$), we use the experimental data of polarizabilities $\alpha_0 = 5.4265a_B^3$ and $\alpha_2 = 1.3567a_B^3$ [26].

C. Phase shifts

The solution of the Calogero equation is used to obtain the scattering phase shifts. The results for different orbital momenta on the basis of the polarization model (7) are shown in Figs. 3–5. We consider the phase-shifts result in Fig. 3. At $k = 0$ the s -wave scattering phase shift $\eta_0(0)$ tends to the value of π . According to the Levinson theorem [40] $\eta(0) = n\pi$ (where n is the number of bound states), it corresponds to one bound state. In our case it is the negative hydrogen molecule. Here H₂⁻ is a metastable state, which appears in reactions such as dissociative attachment (H₂ + $e \rightarrow$ H₂⁻ \rightarrow H + H⁻) and associative attachment (H + H⁻ \rightarrow H₂⁻ \rightarrow H₂ + e). The lifetime of this metastable state was measured to be 5–8 μ s [41]. The theoretical value of the electron affinity (or binding energy) for the bound state H₂⁻ is 2.08×10^{-2} eV/molecule, corresponding to 2 kJ/mol [21]. This value has been taken to calculate the bound part of the second virial coefficient in the Beth-Uhlenbeck formula (2), assuming that H₂⁻ is a resonance.

The phase-shift data for the s channel are compared with the R -matrix data of Ref. [39]. As one can see, the present results for the polarization model (7) are in good agreement

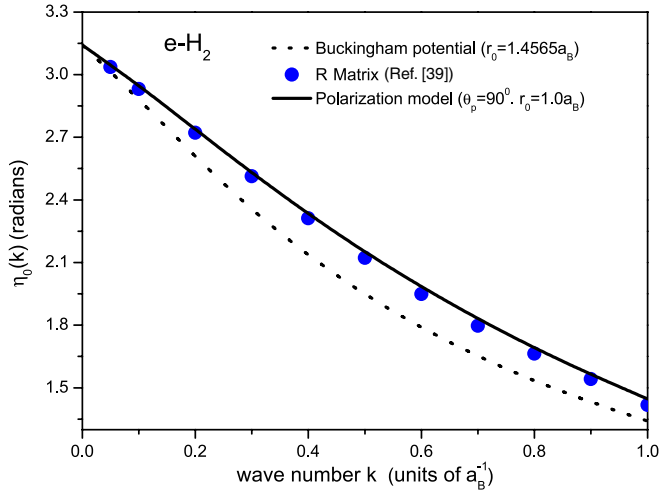


FIG. 3. (Color online) The s -wave scattering phase shifts for e - H_2 . The R -matrix data [39] are compared with the results of the present calculation on the basis of the polarization models (7) and (6).

with Schneider's data. The parameter values of the polarization potential (7) r_0 and θ_p are fit to get good agreement for phase shifts with theoretical data. The cutoff radius in this calculation is taken as $r_0 = 1.0a_B$ and $\theta_p = 90^\circ$. Note that no direct measurements of the phase shifts can be found in the literature, only scattering cross-section data.

In Figs. 4 and 5 the scattering phase shifts for $\ell = 1, 2$ are presented using the same parameters for r_0 and θ_p as for the s wave. Both phase shifts are zero at zero incident energy of the electron since no bound states exist for these scattering channels. The d -wave results are very small in comparison to the s channel at the low-energy limit. In general, to calculate the second virial coefficients the phase shifts for $\ell < 3$ are enough to obtain accurate results. The comparison of p and d waves with Schneider's data [39] shows deviations. This can be explained by the different methods we used and the neglect of symmetry effects in our approach. In the present calculation,

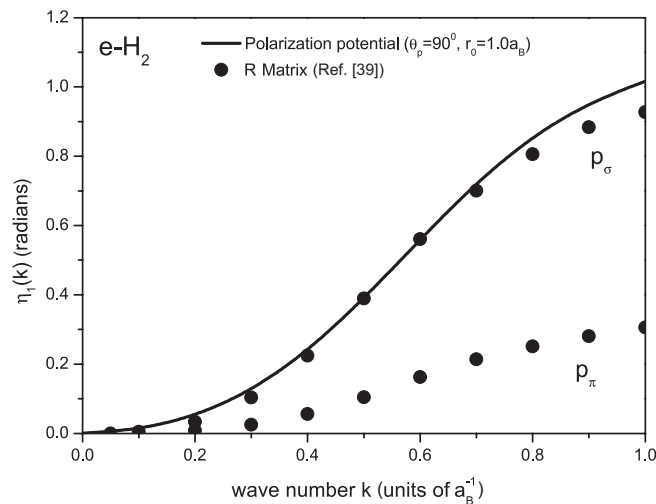


FIG. 4. The p -wave scattering phase shifts for e - H_2 . The R -matrix data [39] are compared with the results of the present calculation on the basis of the polarization model (7).

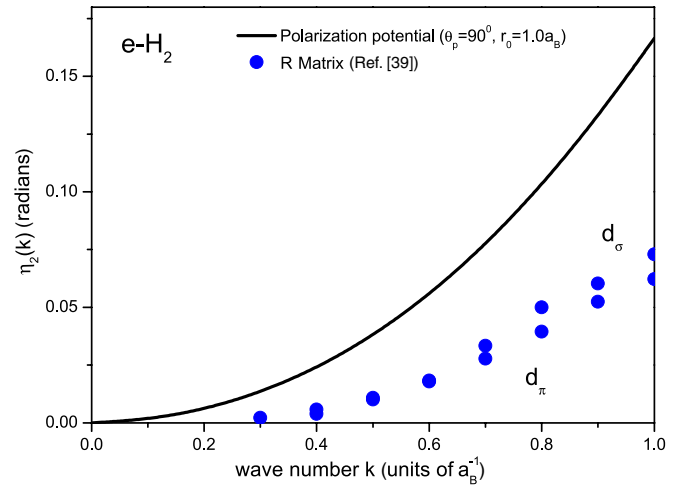


FIG. 5. (Color online) The d -wave scattering phase shifts for e - H_2 . The R -matrix data [39] are compared with the results of the present calculation on the basis of the polarization model (7).

a molecule without structure is considered, so the comparison of data with other theoretical works in σ and π orbitals is not possible. The only confirmation of these studies can be the comparison of the calculated differential cross section with experimental data.

Note that we have not included rotational and vibrational excitations, which leads to an uncertainty in our approach. The adiabatic nucleus approximation (fixed nuclei) was discussed in detail in Ref. [26], comparing theoretical data as well as experimental data from the swarm analysis. Although this is not an issue in this paper, we mention that there are still open questions about vibrational excitations since experiment and theory are in controversy (see, e.g., Refs. [42–44]).

D. Elastic differential cross section

Experimental data for the electron-molecule collisions were collected by Trajmar *et al.* [45], Brunger and Buckman [46], and Yoon *et al.* [25]. The data of Linder and Schmidt (without rotational excitation) were taken to compare this studies' results for differential cross sections. Also, recent experimental data from Muse *et al.* [47] are taken to perform the comparison of differential cross sections.

Using the obtained phase shifts, the differential cross sections can be calculated by the following formula:

$$\frac{dQ(k, \theta)}{d\Omega} = \left| \frac{1}{2ik} \sum_{\ell} (2\ell + 1) [e^{2i\eta_{\ell}^{cd}(k)} - 1] P_{\ell}(\cos \theta) \right|^2, \quad (8)$$

where θ is the scattering angle (do not confuse with θ_p). In our calculation we include the orbital momentum until $\ell = 5$. The dependence of the differential cross section on the scattering angle is shown in Figs. 6–9 for different incident energies of the electron. The experimental data of Muse *et al.* [47] and Linder and Schmidt [28] are compared with the present calculations in Fig. 6. In Fig. 7 the results of the polarization model (7) are compared with the R -matrix data of Schneider [39] and experimental data [28] at $E = 3.4$ eV ($k = 0.5a_B^{-1}$). Our results describe better the collision process

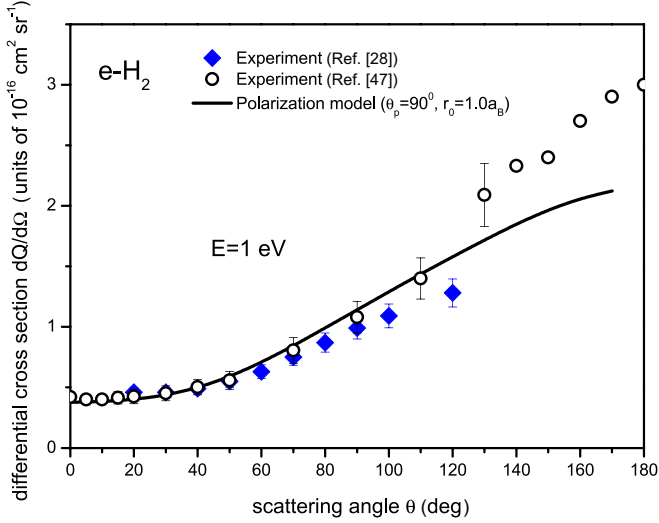


FIG. 6. (Color online) Differential cross sections for $e\text{-H}_2$ at incident energies 1 eV: solid line, calculation with the polarization model (7); diamonds, experimental data from Ref. [28]; circles, experimental data from Ref. [47].

at small scattering angles, whereas the R -matrix data work only at middle angles.

The comparison of our results with experimental data [28,47] at other energies shows good agreement almost at all scattering angles. With increasing incident energy, a slight deviation between experiment and our calculation is observed. It can be explained by an increasing contribution of rotational excitations, which is not included in our calculation. In Fig. 9 also the differential cross section for electron and atom scattering is presented. The atomic cross section, calculated using the Buckingham potential (6), is smaller than the molecular cross section almost by a factor of 2. Although we use a simple approximation to describe the scattering process

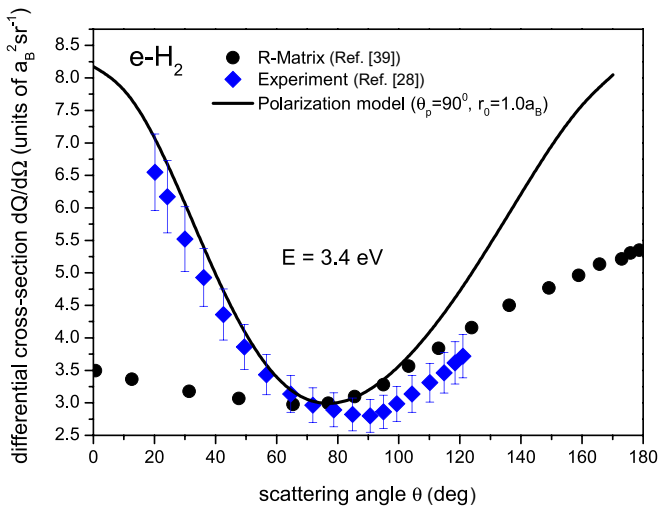


FIG. 7. (Color online) Differential cross sections for $e\text{-H}_2$ at incident energies of 3.4 eV: solid line, calculation with the polarization model (7); diamonds, experimental data from Ref. [28]; circles, experimental data from Ref. [47]; circles, theoretical data from Ref. [39].

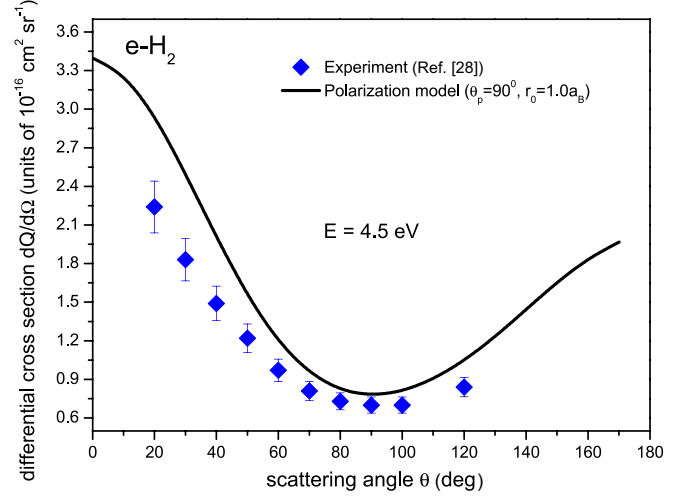


FIG. 8. (Color online) Differential cross sections for $e\text{-H}_2$ at incident energies of 4.5 eV: solid line, calculation with the polarization model (7); diamonds, experimental data from Ref. [28].

between the electron and hydrogen molecule, our results are reliable, which was shown by a comparison with experimental data.

IV. RESULTS AND DISCUSSION

A. Second virial coefficient for the $e\text{-H}_2$ interaction

The data of scattering phase shifts shown in Figs. 3–5, which are based on experimental data, will be used for calculations of the second virial coefficient using the Beth-Uhlenbeck formula (2). The phase shifts are obtained using the polarization model (7). Table II shows results for the normalized second virial coefficients $\tilde{b}_{\text{H}_2-e}^{\text{sc}}$ and $\tilde{b}_{\text{H}_2-e}^{\text{bound}}$ for the

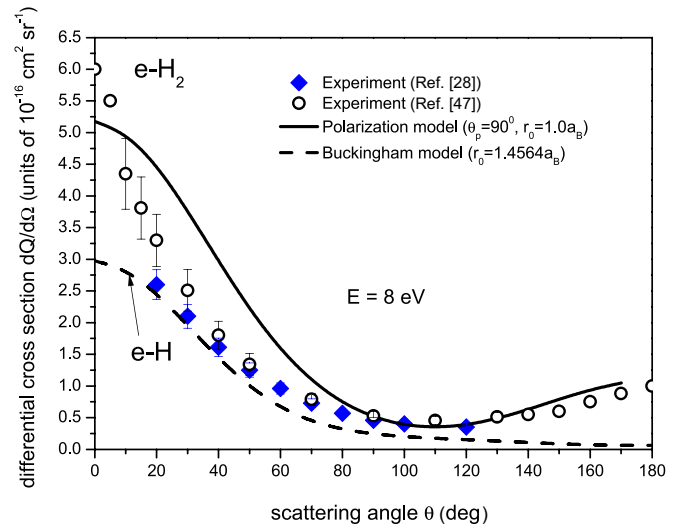


FIG. 9. (Color online) Differential cross sections for $e\text{-H}_2$ at incident energies of 8 eV: solid line, calculation with the polarization model (7); diamonds, experimental data from Ref. [28]; circles, experimental data from Ref. [47]; dashed line, present calculation with the polarization model (6).

TABLE II. Scattering and bound part of the second cluster virial coefficient \tilde{b}_{H_2-e} for different temperatures.

T (K)	$\tilde{b}_{\text{H}_2-e}^{\text{sc}}, s$ wave	$\tilde{b}_{\text{H}_2-e}^{\text{sc}}, p$ wave	$\tilde{b}_{\text{H}_2-e}^{\text{sc}}, d$ wave	$\tilde{b}_{\text{H}_2-e}^{\text{sc}}, \text{full}$	$\tilde{b}_{\text{H}_2-e}^{\text{bound}}$	$\tilde{b}_{\text{H}_2-e}, \text{full}$
5000	0.9308	0.0179	0.0034	0.9522	0.0494	1.0015
7000	0.9173	0.0260	0.0049	0.9499	0.0350	0.9832
8000	0.9113	0.0301	0.0056	0.9482	0.0306	0.9776
9000	0.9056	0.0343	0.0064	0.9464	0.0271	0.9734
10000	0.9002	0.0386	0.0071	0.9460	0.0244	0.9703
11000	0.8951	0.0429	0.0079	0.9460	0.0222	0.9682
12000	0.8903	0.0473	0.0086	0.9462	0.0203	0.9665
13000	0.8856	0.0517	0.0094	0.9468	0.0187	0.9656
14000	0.8813	0.0562	0.0101	0.9476	0.0173	0.9649
15000	0.8770	0.0607	0.0108	0.9485	0.0162	0.9647
20000	0.8576	0.0836	0.0146	0.9560	0.0121	0.9681

scattering and the bound parts, respectively. The second, third, and fourth columns of the table present data for the contribution of the s , p , and d waves to the scattering part of the second virial coefficient, respectively. Higher-order contributions are small and negligible for the temperature range considered here. The $\tilde{b}_{\text{H}_2-e}^{\text{sc}}$ for higher orbital momenta is weaker than for the s wave. With increasing temperature, the scattering part of the second virial coefficient for the s wave decreases weakly, but the results for the other two channels increase. This occurs due to the difference in behavior of phase shifts (see Figs. 3–5). The sixth column shows the bound part (H_2^-) of the second virial coefficient. The bound part decreases with an increase of the temperature. At low temperatures bound particles (clusters) are important. The full second virial coefficient is presented in the last column. The dependence of the full second virial coefficient on temperature is determined by the scattering part. Data from Table II can be used to study thermodynamical properties of the system. Note that the second virial coefficients do not depend on the density of the plasma. The density dependence is included in the virial expansions for thermodynamical functions [see, for instance, the pressure (1)].

B. Ionization equilibrium

The interaction between electrons and neutral clusters can play an essential role for the plasma composition. In a system with charged particles, hydrogen atoms, and hydrogen molecules, the following chemical reactions are possible: $e + i \rightleftharpoons \text{H}$, $\text{H} + \text{H} \rightleftharpoons \text{H}_2$, $e + \text{H} \rightleftharpoons \text{H}^-$, and $e + \text{H}_2 \rightleftharpoons \text{H}_2^-$. Each reaction corresponds to a chemical equilibrium with respect to the chemical potentials, respectively:

$$\begin{aligned}
 \mu_e + \mu_i &= \mu_{\text{H}}, \\
 \mu_{\text{H}} + \mu_{\text{H}} &= \mu_{\text{H}_2}, \\
 \mu_e + \mu_{\text{H}} &= \mu_{\text{H}^-}, \\
 \mu_e + \mu_{\text{H}_2} &= \mu_{\text{H}_2^-}.
 \end{aligned} \tag{9}$$

Note that the clusters H^- and H_2^- are included now as components in the chemical picture. Alternatively, the contribution of these bound states can also be obtained consistently from the Beth-Uhlenbeck formula (2) as a bound-state contribution. Further possible cluster states are not considered in this work;

in particular, the H_2^+ bound state will be obtained in the H- i interaction channel.

In nonideal plasma the chemical potential can be divided into ideal and nonideal parts. For instance, for the chemical potential, the following expression defines the virial coefficients [19]:

$$\mu_c = \mu_c^{\text{id}} - k_{\text{B}}T \left(2 \sum_d n_d b_{cd} + 3 \sum_{de} n_d n_e b_{cde} + \dots \right), \tag{10}$$

where b_{cd} is the second virial coefficient.¹ There is a connection between the dimensionless second virial coefficient \tilde{b}_{cd} [see Eq. (1)] and b_{cd} : $\tilde{b}_{cd} = b_{cd} g_d / \Lambda_d^3$, where g_d is the spin degeneracy factor. The first term of Eq. (10) $\mu_c^{\text{id}} = k_{\text{B}}T \ln(\frac{n_c \Lambda_c^3}{g_c}) + E_c^{(0)}$ is the ideal part of the chemical potential with binding energy $E_c^{(0)}$ of isolated clusters (H , H_2 , H^- , and H_2^-). The nonideal parts $\Delta\mu_{cd}$ are defined by the second virial coefficients b_{cd} and similarly for further terms $\Delta\mu_{cde}$, etc., of Eq. (10). The virial expansion is diverging for Coulomb interactions (for e - e , i - i , and e - i contributions). We need to consider screened interactions and take the classical Debye shift $\Delta_i = -\kappa e^2 / 2$ with the inverse screening length $\kappa^2 = (\frac{4\pi n_i e^2}{k_{\text{B}}T})$ as an approximation for protons. For electrons we use the Padé formulas [10], which can be used at any plasma degeneracy

$$\Delta_e = \frac{\mu_{\text{D}} - (1/2)(\pi\beta)^{-1/2}\bar{n} + 8\bar{n}^2\mu_{\text{GB}}}{1 + 8 \ln[1 + (1/16\sqrt{2})(\pi\beta)^{1/4}\bar{n}^{1/2}] + 8\bar{n}^2}, \tag{11}$$

where $\bar{n} = n_e \Lambda_e^3$, $\mu_{\text{D}} = -(\pi\beta)^{-1/4}\bar{n}^{1/2}$ is the chemical potential in low-density limit (Debye limiting law), and $\mu_{\text{GB}} = -\frac{1.2217}{r_s} - 0.08883 \ln[1 + \frac{6.2208}{r_s^{0.7}}]$ is the Gell-Mann-Brueckner approximation for the highly degenerate region (in Ry), with $r_s = (3/4\pi n_e)^{1/3}/a_{\text{B}}$ the Brueckner parameter.

Finally, using Eqs. (9) and (10), the system of equations can be solved to derive the composition of the plasma with

¹Note that the second virial coefficient as introduced by Beth and Uhlenbeck [18,19] is $-b_2$.

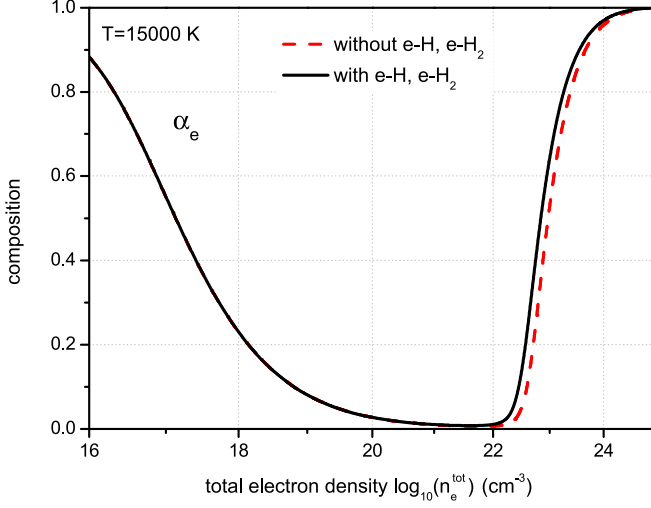


FIG. 10. (Color online) Free-electron-density fraction α_e at $T = 15\,000$ K. The solid line shows the result of the set of equations (12). The dashed line is the result of the set of equations (12) neglecting interaction terms $\Delta\mu_{e-H}^{sc}$ and $\Delta\mu_{e-H_2}^{sc}$.

components e , i , H , H_2 , H^- , and H_2^- ,

$$\begin{aligned} \frac{n_H}{n_e n_i} &= \Lambda_e^3 \exp(-\beta E_0) \exp[\beta(\Delta_e + \Delta_i \\ &\quad - \Delta\mu_{H-H}^{sc} + \Delta\mu_{e-H}^{sc} + \Delta\mu_{e-H_2}^{sc})], \\ \frac{n_{H_2}}{n_H^2} &= b_{H-H}^{\text{bound}} \exp[\beta(2\Delta\mu_{H-H}^{sc} - \Delta\mu_{H_2-H_2}^{sc})], \\ \frac{n_{H^-}}{n_e n_H} &= b_{H-e}^{\text{bound}} \exp[\beta(\Delta_e + \Delta\mu_{H-H}^{sc})], \\ \frac{n_{H_2^-}}{n_e n_{H_2}} &= b_{H_2-e}^{\text{bound}} \exp[\beta(\Delta_e + \Delta\mu_{H_2-H_2}^{sc})], \\ n_e^{\text{tot}} &= n_e + n_H + 2n_{H_2} + 2n_{H^-} + 3n_{H_2^-}, \end{aligned} \quad (12)$$

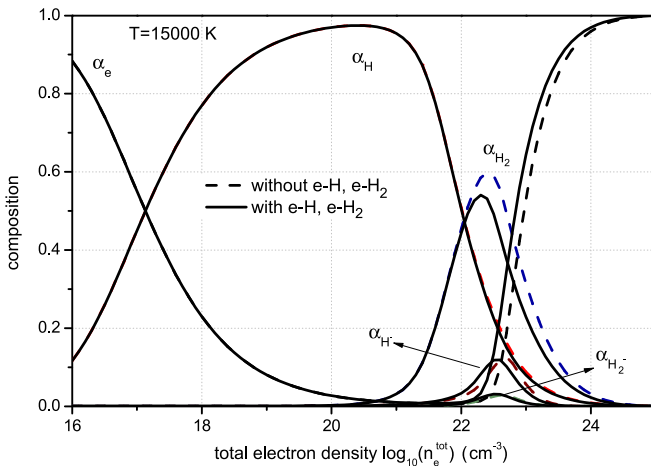


FIG. 11. (Color online) Composition of hydrogen plasma at $T = 15\,000$ K taking into account e , H , H_2 , H^- , and H_2^- constituents. The solid line shows the result of the set of equations (12). The dashed line is the result of the set of equations (12) neglecting interaction terms $\Delta\mu_{e-H}^{sc}$ and $\Delta\mu_{e-H_2}^{sc}$.

TABLE III. Particle-density fractions at $T = 15\,000$ K for e , H , H^- , and H_2^- calculated according to the set of equations (12).

$n_e^{\text{tot}} \text{ (cm}^{-3}\text{)}$	α_e	α_H	α_{H_2}	α_{H^-}	$\alpha_{H_2^-}$
10^{16}	0.883	0.117	1.09×10^{-8}	4.15×10^{-7}	1.32×10^{-13}
10^{18}	0.230	0.770	4.75×10^{-5}	6.94×10^{-5}	1.46×10^{-8}
10^{20}	0.0272	0.964	0.00772	0.000957	2.62×10^{-5}
10^{21}	0.0110	0.891	0.0939	0.00315	0.00112
10^{22}	0.0390	0.381	0.531	0.0202	0.0292

where $E_0 = 13.6$ eV is the ground-state energy of hydrogen. The bound parts of the second virial coefficients are b_{H-H}^{bound} , b_{H-e}^{bound} and $b_{H_2-e}^{\text{bound}}$. The dissociation energy of the hydrogen molecule $D_0 = 4.75$ eV, the vibrational constant $h\nu/k_B = 6338.2$ K [48], and the rotational constant $B = 87.58$ K [48] are included in the bound part of the second virial coefficient

$$b_{H-H}^{\text{bound}} = \frac{1}{\sqrt{2}} \Lambda_H^3 \left(\frac{T}{B}\right) \frac{1}{1 - \exp(-h\nu/k_B T)} \exp(\beta D_0). \quad (13)$$

Here $\Delta\mu_{cd}^{sc} = -2n_d b_{cd}^{sc}/\beta$ is scattering part of the nonideal part of the chemical potential for species c and d . While the rotational and vibrational states are taken into account in the bound part (13), the respective excitations are not considered to be of relevance in the scattering part, following the discussion in Sec. III. The second virial coefficient for the H_2 - H_2 interaction is treated using the hard-core model $b_{H_2-H_2} = \frac{2\pi}{3} d_{H_2}^3(T)$. The diameters of the hydrogen molecule d_{H_2} and b_{H-H}^{sc} are taken from Ref. [10]. Data for the second virial coefficient b_{H-e} can be found in our previous work [17]. The contribution to the second virial coefficient b_{H_2-e} is taken from our calculation (see Table II).

We now focus on the influence of e - H and e - H_2 interactions on the ionization equilibrium. Solutions of the coupled equations (12) at temperature $T = 15\,000$ K are shown in Figs. 10 and 11 in terms of the particle-density fractions $\alpha_e = n_e/n_e^{\text{tot}}$, $\alpha_H = n_H/n_e^{\text{tot}}$, $\alpha_{H_2} = 2n_{H_2}/n_e^{\text{tot}}$, $\alpha_{H^-} = 2n_{H^-}/n_e^{\text{tot}}$, and $\alpha_{H_2^-} = 3n_{H_2^-}/n_e^{\text{tot}}$. Selected data are also given in Tables III and IV. Figure 10 shows the result for the free-electron-density fraction with and without interaction terms $\Delta\mu_{e-H}^{sc}$ and $\Delta\mu_{e-H_2}^{sc}$. Small corrections are observed only at higher densities where pressure ionization sets in. The composition fraction curve is shifted to slightly lower densities due to the additional correlations included. However, looking at a particular density,

TABLE IV. Particle-density fractions at $T = 15\,000$ K for e , H , H^- , and H_2^- calculated according to (12) neglecting interaction terms $\Delta\mu_{e-H}^{sc}$ and $\Delta\mu_{e-H_2}^{sc}$.

$n_e^{\text{tot}} \text{ (cm}^{-3}\text{)}$	α_e	α_H	α_{H_2}	α_{H^-}	$\alpha_{H_2^-}$
10^{16}	0.883	0.117	1.09×10^{-8}	4.15×10^{-7}	1.32×10^{-13}
10^{18}	0.230	0.770	4.75×10^{-5}	6.94×10^{-5}	1.45×10^{-8}
10^{20}	0.0271	0.964	0.00774	0.000967	2.59×10^{-5}
10^{21}	0.00978	0.892	0.0944	0.00379	0.00114
10^{22}	0.00682	0.387	0.566	0.0149	0.0249

for instance, $n = 10^{22} \text{ cm}^{-3}$ (see Tables III and IV), the free-electron-density fraction can change up to 20%. The particle-density fractions of more constituents are shown in Fig. 11. The atomic-density fraction is almost unchanged, but the other density fractions (H_2 , H^- , and H_2^-) are reduced due to the additional correlations taken into account. Additionally, in the density region of 10^{21} – 10^{22} cm^{-3} , the effect of the e - H_2 virial coefficient leads to a decrease of the molecule-density fraction, whereas the fractions of negatively charged carriers (e , H^- , and H_2^-) and positively charged carriers are increased (see Table III and IV).

C. Comparison with the excluded-volume approach

The excluded-volume concept is one of the popular simpler approximations to take the interaction of electrons with neutrals into account [49]. The fraction of volume occupied by atoms can be defined with the filling parameter $\eta = 4/3\pi r_{\text{H}}^3 n_{\text{H}}$, where r_{H} is an atomic radius. The second virial coefficient is given for a system of hard spheres as

$$b_{e\text{-H}}^{\text{ex}} = -\frac{2}{3}\pi r_{\text{H}}^3. \quad (14)$$

The composition of partially ionized hydrogen plasma is calculated by replacing $b_{\text{H-}e}^{\text{sc}}$ in the previous calculations with the second virial coefficient from the excluded-volume concept $b_{e\text{-H}}^{\text{ex}}$ with the hard-core radius of $r_{\text{H}} = 1.0a_{\text{B}}$. Within the considered accuracy, this leads approximately to identical results as for the calculations without an electron-atom interaction (see Table IV). This indicates that the excluded-volume concept with $r_{\text{H}} = 1.0a_{\text{B}}$ makes the interaction of electrons and clusters negligible.

On the other hand, it is interesting to fit the radii of hydrogen atoms and molecules on the basis of the second virial coefficients according to Eq. (14). Using the data for $b_{\text{H-}e}$ from Ref. [17] and for $b_{\text{H}_2\text{-}e}$ from Table II, one can obtain the corresponding radii. Table V shows the results of the fit for different temperatures. The increase of temperature leads to smaller radii. The high energy of projectile electrons leads to fast collisions and closer distances. In the last two columns of Table V, data from Ref. [10] are given. The radii are obtained by the fitting of the classical virial coefficients assuming a real potential for H-H and H_2 - H_2 interactions.

Note that the mean particle distance $d_e = d_i = (3/4\pi n_e^{\text{tot}})^{1/3}$ gives a general limit of applicability of the cluster virial expansion for temperature and density parameters. At the total electron density $n_e^{\text{tot}} = 1.37 \times 10^{22} \text{ cm}^{-3}$ the mean particle distance is $d_e = 4.90a_{\text{B}}$. This means that at $T = 15\,000 \text{ K}$ the use of the second virial coefficients is possible up to this density.

V. CONCLUSION

The cluster virial expansion was applied for the partially ionized hydrogen plasma with molecular components. In particular, the scattering phase shifts of electrons on hydrogen molecules were calculated. The latter were taken as input for

TABLE V. Effective hard-core radius for the hydrogen atom and molecule interacting with electrons. The first two columns show the hard-core radius of the hydrogen atom and molecule according to formula (14). The last two columns are taken from Ref. [10].

T (K)	$r_{\text{H}}/a_{\text{B}}$, full	$r_{\text{H}_2}/a_{\text{B}}$, full	$r_{\text{H}}/a_{\text{B}}$	$r_{\text{H}_2}/a_{\text{B}}$
10000	6.88	8.65		
11000	6.33	8.25		
12000	5.88	7.90		
13000	5.50	7.58		
14000	5.18	7.30		
15000	4.90	7.05	1.50	1.78
20000	3.91	6.12	1.42	1.70
30000	2.91	5.03	1.30	1.57
50000	2.08	3.96		
60000	1.86	3.65		
70000	1.71	3.41		
80000	1.59	3.21		
90000	1.50	3.05		
100000	1.43	2.91		

the Beth-Uhlenbeck formula, which allowed us to calculate the scattering part of the second virial coefficient. Results for the e - H_2 channel were based on the polarization pseudopotential model (7), which was adapted to the experimental data of scattering cross sections. A bound state H_2^- occurs in the bound part of the Beth-Uhlenbeck formula. Alternatively, it can be considered as a different constituent within the chemical picture.

Accurate calculation of the second virial coefficients in a cluster expansion as presented allowed us to describe thermodynamics. In particular, it was possible to obtain the chemical potential, free energy, and equation of state of the partially ionized plasma. The equation of state of plasma is governed by Coulomb contributions. There is only a very limited region where the formation of H_2 is appreciable. Then the H_2 - e interaction is relevant and gives a contribution (see Fig. 11). Usually, a hard-core approach is considered to estimate this contribution. We have shown that a more systematic approach, which is based on microscopic processes, is possible. An accurate value for the second e - H_2 virial coefficient is necessary if high-precision experiments are performed in the region of coexistence of both components.

Improvements of the second virial coefficients should include vibrational and rotational excitational channels in the scattering theory. The influence of the excitational channels on the equation of state is a task for future studies. It would also be of interest to extend our method to conditions of nonequilibrium.

ACKNOWLEDGMENT

This work was supported by the German Research Foundation (DFG) under Grant No. SFB 652 “Strong Correlations and Collective Effects in Radiation Fields: Coulomb Systems, Clusters and Particles.”

- [1] J. Lewis, *Physics and Chemistry of the Solar Systems* (Elsevier, Amsterdam, 2004).
- [2] R. Redmer, in *Plasma Physics*, edited by A. Dinklage, T. Klinger, G. Marx, and L. Schweikhard, Lecture Notes in Physics Vol. 670 (Springer, Berlin, 2005), p. 331.
- [3] R. Redmer, B. Holst, H. Juranek, N. Nettelmann, and V. Schwarz, *J. Phys. A: Math. Gen.* **39**, 4479 (2006).
- [4] R. Redmer, *Plasma Physics. Confinement, Transport and Collective Effects* (Springer, Berlin, 2005).
- [5] W. Lorenzen, B. Holst, and R. Redmer, *Phys. Rev. Lett.* **102**, 115701 (2009).
- [6] J. Vorberger, M. Schlanges, and W. D. Kraeft, *Phys. Rev. E* **69**, 046407 (2004).
- [7] R. P. Drake, *High-Energy-Density Physics* (Springer, New York, 2006).
- [8] J. D. Lindl, P. Amendt, R. L. Berger *et al.*, *Phys. Plasmas* **11**, 339 (2004).
- [9] H. Fehske, R. Schneider, and A. Weisse, *Computational Many-Particle Physics* (Springer, Berlin, 2008), Vol. 739.
- [10] D. Kremp, M. Schlanges, and W.-D. Kraeft, *Quantum Statistics of Nonideal Plasmas* (Springer, Berlin, 2005).
- [11] D. Saumon, G. Chabrier, and H. M. V. Horn, *Astrophys. J. Suppl. Ser.* **99**, 713 (1995).
- [12] G. I. Kerley, Equations of state for hydrogen and deuterium, Sandia Report No. SAND2003-3613, 2003 (unpublished).
- [13] W. D. Kraeft, D. Kremp *et al.*, *Quantum Statistics of Charged Particle Systems* (Springer, Berlin, 1986).
- [14] B. Holst, R. Redmer, V. Gryaznov, V. Fortov, and I. Iosilevskiy, *Eur. Phys. J. D* **66**, 104 (2012).
- [15] A. Alastuey and A. Perez, *Phys. Rev. E* **53**, 5714 (1996).
- [16] B. Militzer and D. M. Ceperley, *Phys. Rev. E* **63**, 066404 (2001).
- [17] Y. A. Omarbakiyeva, C. Fortmann, T. S. Ramazanov, and G. Röpke, *Phys. Rev. E* **82**, 026407 (2010).
- [18] E. Beth and G. E. Uhlenbeck, *Physica* **4**, 915 (1937).
- [19] K. Huang, *Statistical Mechanics* (Wiley, New York, 1966).
- [20] F. J. Rogers and A. Nayfonov, *Astrophys. J.* **576**, 1064 (2002).
- [21] R. Harcourt, *J. Phys. B* **20**, L617 (1987).
- [22] J. Liu, E. Salumbides *et al.*, *J. Chem. Phys.* **130**, 174306 (2009).
- [23] S. Trajmar, D. Truhlar, and J. Rice, *J. Chem. Phys.* **52**, 4502 (1970).
- [24] D. E. Golden, H. W. Bandel, and J. A. Salerno, *Phys. Rev.* **146**, 40 (1966).
- [25] J.-S. Yoon, M.-Y. Song, J.-M. Han, S. H. Hwang, W.-S. Chang, B. Lee, and Y. Itikawa, *J. Phys. Chem. Ref. Data* **37**, 913 (2008).
- [26] M. A. Morrison, R. W. Crompton, B. C. Saha, and Z. L. Petrovic, *Aust. J. Phys.* **40**, 239 (1987).
- [27] R. W. Crompton, D. K. Gibson, and A. I. McIntosh, *Aust. J. Phys.* **22**, 715 (1969).
- [28] F. Linder and H. Schmidt, *Z. Naturforsch. A* **26**, 1603 (1971).
- [29] N. F. Lane, *Rev. Mod. Phys.* **52**, 29 (1980).
- [30] T. F. Malley, L. Spruch, and L. Rosenberg, *J. Math. Phys.* **2**, 491 (1961).
- [31] T. F. Malley, L. Rosenberg, and L. Spruch, *Phys. Rev.* **125**, 1300 (1962).
- [32] K. Fedus, Z. Idziaszek, and G. P. Karwasz, *Eur. Phys. J. ST* **222**, 2335 (2013).
- [33] G. P. Karwasz, R. S. Brusa, and A. Zecca, in *Photon and Electron Interactions with Atoms, Molecules and Ions* (Springer, New York, 2003).
- [34] F. Calogero, *Variable Phase Approach to Potential Scattering* (Academic, New York, 1967).
- [35] V. V. Babikov, *The Method of Phase Functions in Quantum Mechanics* (Nauka, Moscow, 1988).
- [36] Y. A. Omarbakiyeva, G. Röpke, and T. S. Ramazanov, *Contrib. Plasma Phys.* **49**, 718 (2009).
- [37] R. Redmer, G. Röpke, and R. Zimmermann, *J. Phys. B* **20**, 4069 (1987).
- [38] R. Redmer, *Phys. Rep.* **282**, 35 (1997).
- [39] B. I. Schneider, *Phys. Rev. A* **11**, 1957 (1975).
- [40] N. Levinson, K. Dan. Vidensk. Selsk, *Mat. Fys. Medd.* **25**, 1 (1949).
- [41] B. Jordan-Thaden *et al.*, *Phys. Rev. Lett.* **107**, 193003 (2011).
- [42] S. J. Buckman, M. J. Brunger, D. S. Newman, G. Snitchler, S. Alston, D. W. Norcross, M. A. Morrison, B. C. Saha, G. Danby, and W. K. Trail, *Phys. Rev. Lett.* **65**, 3253 (1990).
- [43] Z. L. Petrovic and R. W. Crompton, *Aust. J. Phys.* **40**, 347 (1987).
- [44] J. P. England *et al.*, *Aust. J. Phys.* **41**, 573 (1988).
- [45] S. Trajmar, D. Register, and A. Chutjian, *Phys. Rep.* **97**, 219 (1983).
- [46] M. J. Brunger and S. J. Buckman, *Phys. Rep.* **357**, 215 (2002).
- [47] J. Muse, H. Silva *et al.*, *J. Phys. B* **41**, 095203 (2008).
- [48] K. P. Huber and G. Herzberg, *Molecular Spectra and Molecular Structure. IV. Constants of Diatomic Molecules* (Van Nostrand Reinhold, New York, 1979).
- [49] W. Ebeling, A. Foerster, V. E. Fortov, V. K. Gryaznov, and Y. Polischchuk, *Thermophysical Properties of Hot Dense Plasmas* (Teubner, Stuttgart, 1991).